

Article

Estimation of Reference Evapotranspiration in a Semi-Arid Region of Mexico

Gerardo Delgado-Ramírez ¹, Martín Alejandro Bolaños-González ^{1,*}, Abel Quevedo-Nolasco ¹, Adolfo López-Pérez ¹  and Juan Estrada-Ávalos ²

¹ Hydrosociences, Postgraduate College, Campus Montecillo, México-Texcoco Highway Km 36.5, Montecillo 56264, Mexico; delgado.gerardo@colpos.mx (G.D.-R.); anolasco@colpos.mx (A.Q.-N.); adolfholp@colpos.mx (A.L.-P.)

² National Institute for Forest, Agriculture and Livestock Research (INIFAP), National Center for Disciplinary Research on Water, Soil, Plant and Atmosphere Relationships (CENID-RASPA), Right Bank Sacramento Channel Km 6.5, Gómez Palacio 35150, Mexico; estrada.juan@inifap.gob.mx

* Correspondence: bolanos@colpos.mx

Abstract: Reference evapotranspiration (ET_0) is the first step in calculating crop irrigation demand, and numerous methods have been proposed to estimate this parameter. FAO-56 Penman–Monteith (PM) is the only standard method for defining and calculating ET_0 . However, it requires radiation, air temperature, atmospheric humidity, and wind speed data, limiting its application in regions where these data are unavailable; therefore, new alternatives are required. This study compared the accuracy of ET_0 calculated with the Blaney–Criddle (BC) and Hargreaves–Samani (HS) methods versus PM using information from an automated weather station (AWS) and the NASA-POWER platform (NP) for different periods. The information collected corresponds to Module XII of the Lagunera Region Irrigation District 017, a semi-arid region in the North of Mexico. The HS method underestimated the reference evapotranspiration (ET_0) by 5.5% compared to the PM method considering the total ET_0 of the study period (26 February to 9 August 2021) and yielded the best fit in the different evaluation periods (daily, 5-day mean, and 5-day cumulative); the latter showed the best values of inferential parameters. The information about maximum and minimum temperatures from the NP platform was suitable for estimating ET_0 using the HS equation. This data source is a suitable alternative, particularly in semi-arid regions with limited climatological data from weather stations.

Keywords: NASA-POWER platform; empirical equations; reanalysis data; meteorological data



Citation: Delgado-Ramírez, G.; Bolaños-González, M.A.; Quevedo-Nolasco, A.; López-Pérez, A.; Estrada-Ávalos, J. Estimation of Reference Evapotranspiration in a Semi-Arid Region of Mexico. *Sensors* **2023**, *23*, 7007. <https://doi.org/10.3390/s23157007>

Academic Editor: Alla Yurova

Received: 29 June 2023

Revised: 31 July 2023

Accepted: 1 August 2023

Published: 7 August 2023



Copyright: © 2023 by the authors. Licensee MDPI, Basel, Switzerland. This article is an open access article distributed under the terms and conditions of the Creative Commons Attribution (CC BY) license (<https://creativecommons.org/licenses/by/4.0/>).

1. Introduction

Evapotranspiration (ET) is the sum of transpiration through the plant canopy and evaporation from the soil, plant, and free surface water [1,2]. ET is the most significant component of the hydrological cycle [1,3], due to which its estimation is of common interest in climatological, hydrological, forestry, and agricultural studies [4]. This last area ET is a fundamental variable for calculating water requirements, making efficient use of water in crop production [5]. ET can be measured directly using weighing lysimeters or by measuring the net flux of water vapor between the surface and the surrounding atmosphere using micrometeorological methods [6], which depend on the energy balance of the canopy and include the energy balance of Bowen's relation, eddy covariance, and the use of scintillometers [7].

Crop evapotranspiration (ET_C) is a crucial aspect of the water balance in agricultural areas. To estimate it, the most accessible method is to estimate reference evapotranspiration (ET_0) and then pair it with crop and soil coefficients [8]. Reference evapotranspiration (ET_0) is the evapotranspiration rate of a hypothetical reference crop (grass or alfalfa) with a height of 0.12 m, a fixed surface resistance of 70 s m^{-1} , and an albedo of 0.23, homogeneous, well-watered, free from diseases and pests, growing vigorously, and providing complete

shade to the soil [9–11]. ET_0 measures atmospheric evaporation demand regardless of crop type, development, and management practices [12,13]. This variable is affected only by climatic factors [14] and can be calculated from meteorological data [10].

Estimating ET_0 is the first step in designing, planning, and managing different irrigation systems [15,16]. In addition, it is relevant for calculating crop water requirements [17,18]. This parameter is the backbone of the agronomic design of any irrigation system, facilitates its operation (irrigation schedule and shifts), and allows the planning of water resource management in a basin [19] or an irrigation district. Therefore, its accurate estimation is essential in water management, particularly in arid and semi-arid areas where water is scarce [20].

Given its importance, and the climate's temporal and spatial variability, many models to estimate ET_0 have been proposed. In general, the models available in the published literature can be broadly classified as follows: (1) fully physically based models on a combination of energy balance and mass transfer; (2) semi-physical models based on temperature, radiation, and evaporation data; and (3) black-box models based on artificial neural networks, empirical relationships, and genetic and fuzzy algorithms [21,22].

Due to its practicality, many empirical equations have been developed from field experiments and those based on theoretical approaches [19]. These methods include the evaporimeter tank and empirical equations, including the complete physical model (FAO-56 Penman–Monteith), the equation based on temperature (Blaney–Criddle, Thornthwaite, and Turc), and the one based on temperature and radiation (Hargreaves, Jensen–Haise, Priestley–Taylor, and FAO Radiation), among others [21].

The UN Food and Agriculture Organization (FAO) recommends the Penman–Monteith standard method described in the FAO-56 Manual because it can be used in arid, temperate, and tropical areas [23]. Furthermore, this standardized method is more accurate than the standard proposed by the American Society of Civil Engineers (ASCE), ASCE-PM, when estimating daily ET_0 ; both ways were compared with lysimetric measurements [24]. However, this method requires various meteorological input variables (temperature, solar radiation, relative humidity, and wind speed), which restrains its widespread use [25]. Therefore, its usefulness is limited in regions with no meteorological stations or a shortage of input data [26], which are usually unavailable with the required frequency and quality [27]. The other equations can be used in regions with very little climatological information, such as the case of Hargreaves–Samani (HS) and Blaney–Criddle (BC) equations, which are the most common ones [28–30] and only require temperature as an input variable [31].

The accuracy of the HS and BC equations has been evaluated by several authors, comparing their results with the FAO-56 Penman–Monteith (PM) reference method; HS was the equation that attained the best fit in semi-arid regions [32,33]. Other authors state that the HS method works well in most climatic regions, except for wet areas where it tends to overestimate ET_0 [16,34–36]. Since HS was developed empirically based on data from arid to subhumid environments, it may not fit well to conditions markedly different from those considered for its calibration, as is the case of wet climates [16]. On the other hand, the HS method underestimates ET_0 for dry and windy areas because it does not include wind and is seemingly more accurate when applied for 5- to 7-day averages than for daily time scales [37,38]. However, despite a reasonably good performance of the HS equation in most applications, particularly irrigation planning, several authors have attempted to either recalibrate the HS coefficients or parameters [36,39] or modify the equation itself [40,41], aiming to improve its performance.

Reanalysis data or gridded meteorological data are an alternate source of information that can be used to estimate ET_0 [42–44]. It is available on different platforms: National Aeronautics and Space Administration—Prediction of Worldwide Energy Resource (NASA-POWER) [27,45], Global Land Data Assimilation System (GLDAS) [46], Climate Forecast System ver. 2 (CFSv2) [47], North American Land Data Assimilation System (NLDAS) [48], and National Digital Forecast Database (NDFD) [49]. These global or regional platforms provide data with higher spatial and temporal resolution [27]. However, it should be noted

that higher spatial resolution does not necessarily imply higher precision [50]. The NASA-POWER platform (NP) is the most widely used to estimate ET_0 [51–53]. NP provides daily information on air temperature, precipitation, relative humidity, radiation, wind direction, and speed; it is free and easily accessible. This information is grouped into three different spatial conditions: for a single point, with time series data available based on registered geographic coordinates chosen by the user; at the regional level, in a time series dataset based on a bounding box of user-determined geographic coordinates; and globally, with climate averages worldwide [54]. Despite the wide availability of information and ease of access, evaluating and validating said NP climate information with in situ weather stations in the area of interest is essential for local bias correction and to improve accuracy [45].

This study aims to compare the accuracy of ET_0 calculated with the BC and HS methods relative to the FAO-56 Penman–Monteith (PM) reference method, with data recorded by an automated weather station (AWS) and temperature data (maximum and minimum) from the NASA–POWER platform (NP), for different calculation periods.

2. Materials and Methods

2.1. Study Area and Data Collection

The climatic variables to calculate ET_0 with empirical equations were recorded with a wireless Davis Vantage Pro 2 Plus AWS (Davis Instruments Company, Hayward, CA, USA); it has a console that allows viewing of all meteorological variables simultaneously [55], with a 30-min update frequency.

The AWS belongs to Centro Nacional de Investigación Disciplinaria en Relación Agua, Suelo, Planta, Atmósfera (National Center for Disciplinary Research on Water, Soil, Plant, Atmosphere; CENID RASPA) of Instituto Nacional de Investigaciones Forestales, Agrícolas y Pecuarias (National Institute of Forestry, Agricultural, and Livestock Research; INIFAP), within the facilities of an agricultural production unit located at Module XII of the Lagunera Region Irrigation District 017, at 1110 m a.s.l. and coordinates $25^{\circ}47'00.32''$ N, $103^{\circ}18'46.54''$ W (Figure 1).

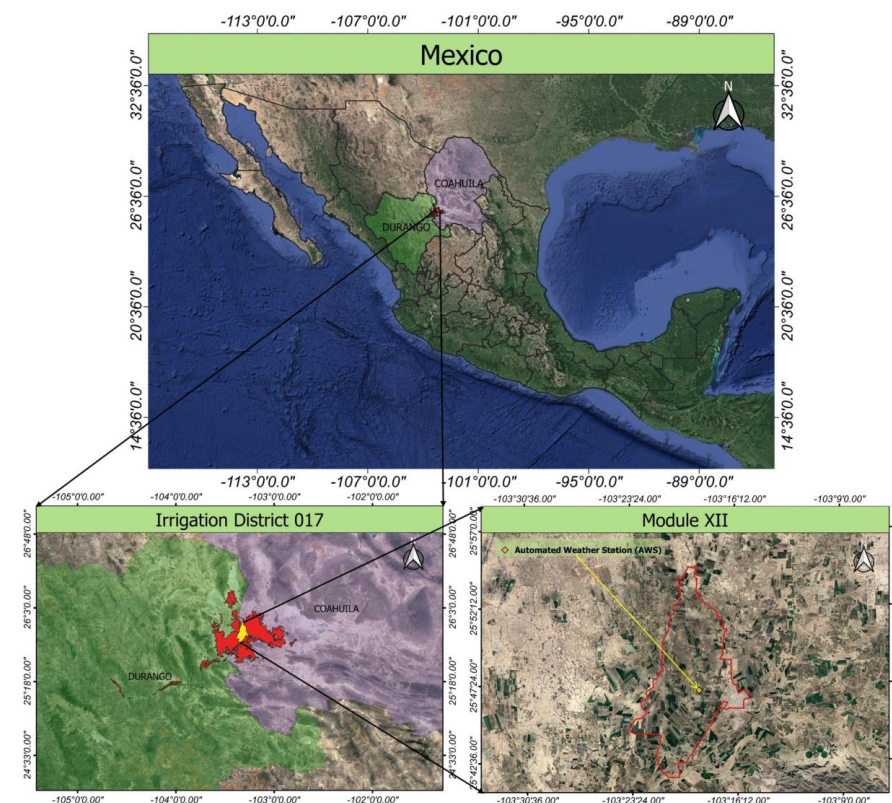


Figure 1. Location of the automated weather station (AWS).

Module XII covers an area of 14,276.7 hectares with an elevation range of 1102 to 1114 m [56]. The slope of the area is gentle, at around 0.06%. It is oriented from south to north, with the southern part being the highest, as shown in Figure 2.

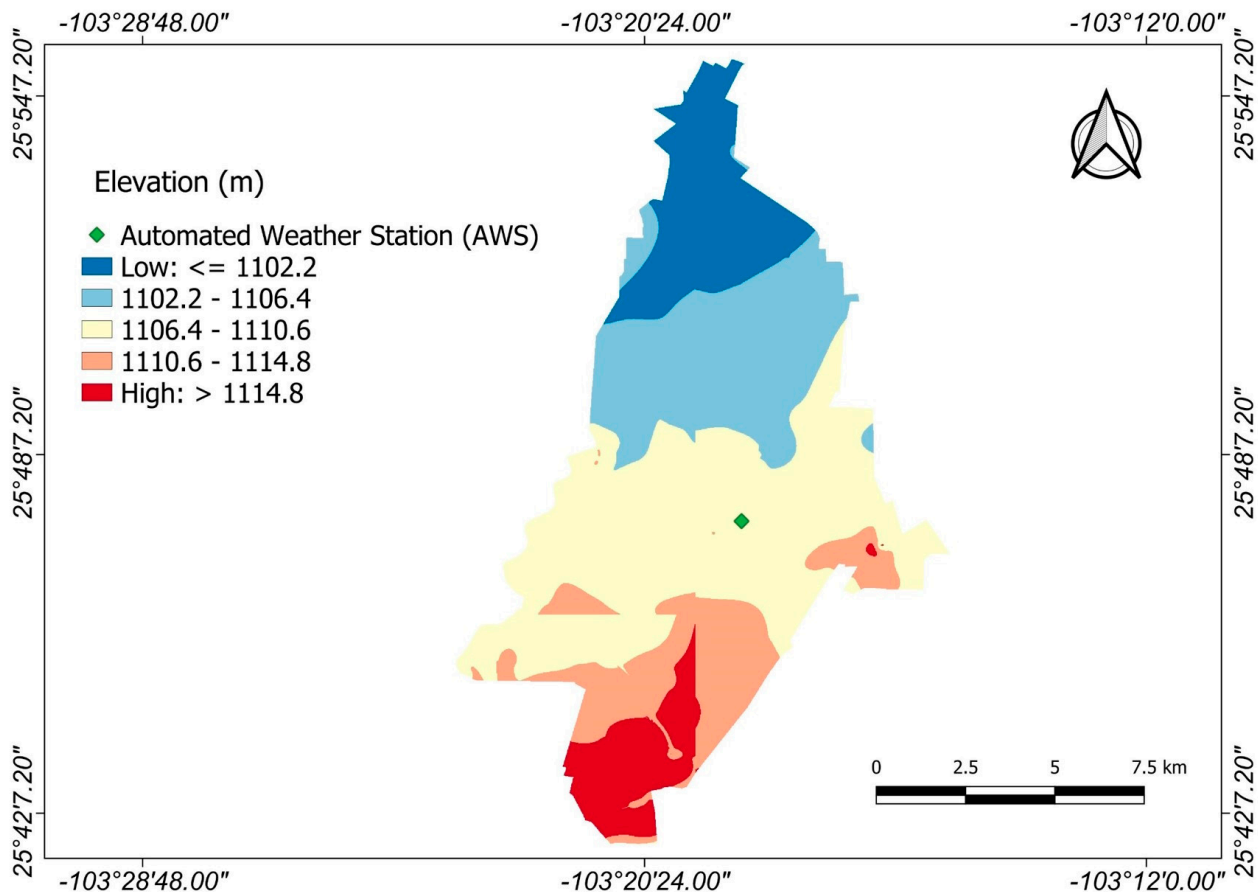


Figure 2. Altitude map of Module XII.

Based on data gathered from Series VII of INEGI (2018) [57], it is estimated that the study area is primarily used for irrigated agriculture, with 89.3% of its surface area dedicated to this use. Human settlements make up 8.7% of the area, while the remaining 2% is used for other purposes (Table 1).

Table 1. Land use and vegetation of the study area INEGI-Series VII (2018).

Land Use	Code	Surface (ha)	Coverage (%)
Human Settlements	AH	1240.1	8.69
Barren Land	DV	15.6	0.11
Annual and Semi-permanent Irrigated Agriculture	RAS	10,166.6	71.21
Permanent Irrigated Agriculture	RP	63.0	0.44
Semi-permanent Irrigated Agriculture	RS	2521.3	17.66
Microphyllous Desert Scrub with Secondary Shrub Vegetation	Vsa/MDM	237.1	1.66
Halophilous Xerophytic Vegetation with Secondary Shrub Vegetation	Vsa/VH	32.9	0.23
Total		14,276.7	100.00

The meteorological information used was daily averages for the period between 26 February (Julian day 57) and 9 August (Julian day 221) 2021 ($n = 165$). In the Lagunera Region Irrigation District 017, the main crops of the spring–summer cycle are grown in this period, including forage corn.

In addition, the meteorological variables were downloaded from the NP climate website (National Aeronautics and Space Administration—Prediction of Worldwide Energy Resource; <https://power.larc.nasa.gov>, accessed on 5 October 2022). This website collects information from various sources: data recorded on-site, satellite data, wind probes, and assimilated data systems [27].

The NNP weather data are based on a single assimilation model named GMAO (Global Modeling and Assimilation Office), starting from the MERRA-2 (Modern Era Retrospective-Analysis for Research and Applications) reanalysis dataset and the GEOS (Goddard Earth Observation System) data processing system [58,59]. Solar radiation is derived from the GEWEX SRB (Global Energy and Water Exchanges Project Surface Radiation Budget) project [60,61].

The horizontal resolution of the NP meteorological data source corresponds to a $\frac{1}{2}^\circ \times 5/8^\circ$ latitude/longitude grid, and the solar data sources come from a $1^\circ \times 1^\circ$ latitude/longitude grid. The current version no longer reassigns data to a common grid; once the data are processed and filed, they are available through the NP service package. The meteorological data is derived from NASA's GMAO MERRA-2 and GEOS 5.12.4 FP-IT. The NP platform team processes GEOS data daily and combines them with MERRA-2 data, producing daily time series that yield low-latency products usually available in approximately two days (real-time). Energy flow data (solar irradiance, thermal IR, and cloud properties) derive from NASA's GEWEX SRB Release 4-Integrated Product (R4-IP) file and CERES SYNIdex and FLASHFlux projects. These data are processed daily and added to the daily time series, issuing products after approximately 4 days, almost in real-time [62].

The main features of the NP system database are shown in Table 2. The AWS is situated near the center of Module XII (Figure 2) and aligns with the center of the NP platform cell. This suggests that one cell encompasses the entire study area's surface.

Table 2. Features of the NASA-POWER (NP) system information.

Parameter	Feature
Data period	1981 to date
Geographic range	Global
Download format	ASCII, CSV, GeoJSON, and NetCDF
Temporal resolution	Daily
Spatial resolution	$0.5^\circ \times 0.5^\circ$ (55.56 km \times 55.56 km cell) for temperature (T), relative humidity (RH), and wind speed (u_2). $1.0^\circ \times 1.0^\circ$ for solar radiation and extraterrestrial solar radiation data.
Delayed data availability	Approximately two days for temperature, relative humidity, and wind speed, and five days for solar radiation data.

2.2. ET_0 Estimation with Empirical Equations

ET_0 was estimated through three empirical equations with different information requirements: an equation based on a complete physical model (PM); another on temperature and solar radiation (HS); and the last one on temperature, relative humidity, and wind speed (BC).

2.2.1. FAO-56 Penman–Monteith Method (ET_0 -PM)

ET_0 was estimated daily with the FAO-56 Penman–Monteith method using Equation (1) [22,63]; this method is useful for arid, temperate, and tropical zones [19,22].

$$ET_{0-PM} = \frac{0.408\Delta(R_n - G) + \gamma \frac{900}{T+273} u_2 (e_s - e_a)}{\Delta + \gamma(1 + 0.34u_2)}, \quad (1)$$

where R_n is the net radiation at the reference crop surface ($\text{MJ m}^{-2} \text{d}^{-1}$); G is the soil heat flux density ($\text{MJ m}^{-2} \text{d}^{-1}$); u_2 is the wind speed at 2 m height (m s^{-1}); e_s is the saturation vapor pressure (kPa); e_a is the actual vapor pressure (kPa); $e_s - e_a$ is the vapor

pressure deficit (kPa); Δ is the slope of the vapor saturation pressure curve (kPa °C⁻¹); T is the mean daily air temperature at 2 m height (°C); and γ is the psychrometric constant (kPa °C⁻¹). For daily time intervals, G values are relatively small, and therefore, this term was not included [22].

2.2.2. Hargreaves–Samani Method (ET₀-HS)

The Hargreaves–Samani method estimates ET₀ based on temperature data only (Equation (2)) [64]. This equation was developed for semi-arid zones and is useful when solar radiation data are not available; however, as it is based on a few variables, its accuracy should be evaluated at the regional and local levels [65].

$$ET_{0-HS} = K_H(T + K_T)R_0 \times (T_{max} - T_{min})^{A_H}, \quad (2)$$

where T is the mean daily air temperature (°C); R_0 is the extraterrestrial solar radiation (from tables, mm d⁻¹); T_{max} is the maximum daily air temperature (°C); T_{min} is the minimum daily air temperature (°C); K_H and K_T are the empirical calibration parameters; and A_H is a Hargreaves' empirical exponent. This study used the original values proposed by Hargreaves and Samani [64]: $K_H = 0.0023$, $K_T = 17.78$, and $A_H = 0.5$.

2.2.3. Blaney–Criddle Method (ET₀-BC)

The meteorological variables required to apply the Blaney–Criddle method are air temperature, relative humidity, and daytime wind speed (Equation (3) [66]).

$$ET_{0-BC} = a + b[p(0.46 \times T + 8.13)], \quad (3)$$

where a and b are climatic calibration coefficients calculated with Equations (4) and (5), respectively; p is the mean annual percentage of daytime hours (value from tables, decimal); and T is the mean air temperature at 2 m height (°C).

$$a = 0.0043 \times RH_{min} - \frac{n}{N} - 1.41, \quad (4)$$

where RH_{MIN} is the minimum relative humidity (%); $\frac{n}{N}$ is the ratio between theoretical and actual sunlit hours (value from tables, decimal).

$$b = 0.082 - 0.0041(RH_{min}) + 1.07\left(\frac{n}{N}\right) + 0.066(u_2) - 0.006(RH_{min})\left(\frac{n}{N}\right) - 0.0006(RH_{min})(u_2), \quad (5)$$

where u_2 is the mean daily wind speed at 2 m height (m s⁻¹).

2.3. Inferential Evaluation Parameters

Table 3 shows the inferential parameters used for evaluating the empirical equations that estimate ET₀ (HS and BC), considering the PM method as a reference. Likewise, the climatic information of the NP platform was evaluated when calculating ET₀ through the reference method (PM_{NP}).

In the above equations, E_i is the estimated value using the empirical equation; O_i is the value obtained with the reference method; \bar{E} is the average of estimated values obtained with the empirical equation; \bar{O} is the average of the values obtained with the reference method; and n is the number of observations. The criteria for interpreting the reliability coefficient are cited in [67].

ET₀ was estimated in three different ways with empirical equations (daily, mean, and cumulative) using a total of 165 observations. The mean ET₀ was determined over the 5-day period, as was the cumulative.

Table 3. Equations and optimal values of inferential parameters.

Parameter	Equation	Optimal Value
Coefficient of Determination (R^2)	$R^2 = \frac{[\sum_{i=1}^n (E_i - \bar{E})(O_i - \bar{O})]^2}{\sum_{i=1}^n (E_i - \bar{E})^2 \sum_{i=1}^n (O_i - \bar{O})^2}$ (6)	1
Root Mean Error (RMSE)	$RMSE = \sqrt{\frac{\sum_{i=1}^n (E_i - O_i)^2}{n}}$ (7)	0
Estimate Error Percentage (PE)	$PE = \left \frac{\bar{E} - \bar{O}}{\bar{O}} \right * 100$ (8)	0
Mean Error Bias (MBE)	$MBE = \frac{\sum_{i=1}^n (E_i - O_i)}{n}$ (9)	0
Concordance Index (d)	$d = 1 - \left[\frac{\sum_{i=1}^n (E_i - O_i)^2}{\sum_{i=1}^n (E_i - \bar{O} + O_i - \bar{O})^2} \right]$ (10)	1
Correlation coefficient (r)	$r = \frac{\sum_{i=1}^n (O_i - \bar{O})(E_i - \bar{E})}{\sqrt{\sum_{i=1}^n (O_i - \bar{O})^2} \sqrt{\sum_{i=1}^n (E_i - \bar{E})^2}}$ (11)	1
Reliability coefficient (c)	$c = r * d$ (12)	1
Regression coefficient (b)	$b = \frac{\sum_{i=1}^n O_i E_i}{\sum_{i=1}^n O_i^2}$ (13)	1

3. Results and Discussion

The daily ET_0 calculated by the PM method and with AWS meteorological data (Figure 3) had the peak value (8.8 mm d^{-1}) on Julian day 126 (6 May 2021)—on the same day, a wind speed of 5.0 m s^{-1} was recorded, which was higher than the average recorded over the study period (2.2 m s^{-1}). On the other hand, the minimum ET_0 (2.2 mm day^{-1}) was recorded on Julian day 192 (11 July 2021)—the day that recorded a solar radiation value of 107.0 W m^{-2} , lower than the average for the study period (282.8 W m^{-2}). This low radiation was due to atypical conditions: high cloudiness (rainfall of 7.6 mm recorded) and high relative humidity (84.5%). Some authors mention that wind speed and solar radiation are the climatic variables with the most significant influence on ET_0 estimates in the study area [27]. Other authors reach the same conclusion when performing a sensitivity analysis in other regions [68–70].

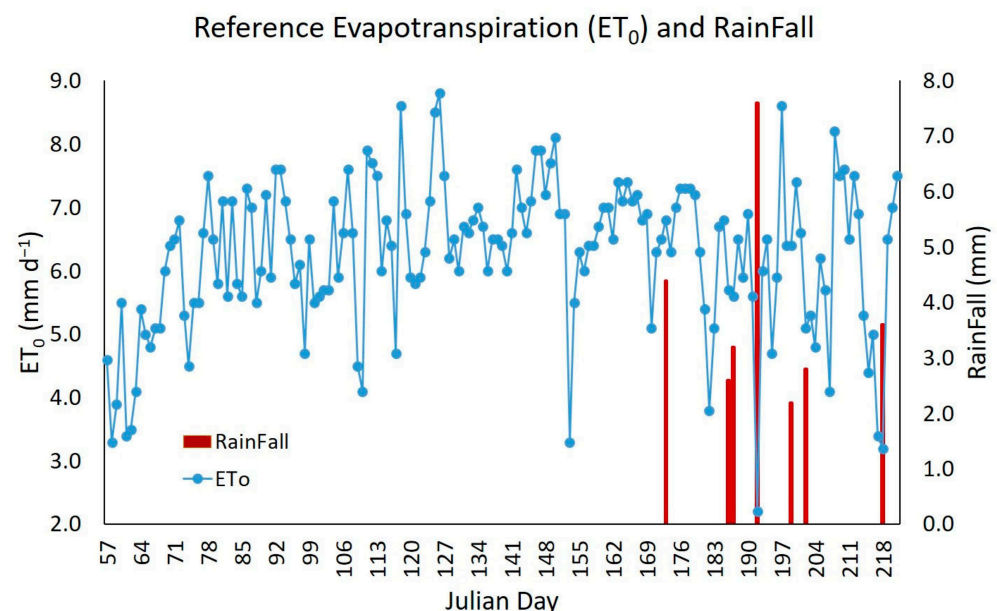


Figure 3. Reference evapotranspiration estimated with the FA0-56 Penman–Monteith method using AWS meteorological data (blue points) and rainfall recorded in the study period (red bars).

3.1. Comparison of ET_0 Estimated by Empirical Equations versus the Reference Method

Table 4 shows the monthly and total ET_0 estimated using the empirical equations and the reference method (PM). Considering the month with the maximum ET_0 (May, with the HS and PM_NP equations and June with the BC method) and the reference method (PM), HS yielded an ET_0 value that was 6.6% lower vs. PM; BC, 12.5% lower; and PM_NP,

13.2% higher. However, considering the month with the minimum ET_0 (February) and the PM method, HS yielded an ET_0 12.8% higher vs. PM; BC, 6.8% higher; and PM_NP, 14.2% higher. It is observed that HS and BC underestimate ET_0 over most of the study period, consistent with the findings reported by some authors for an agroclimatic region similar to the study area [71].

Table 4. Monthly and total ET_0 estimated by empirical equations and the reference method (FAO-56 Penman–Monteith) during the study period.

Variable	Evaluation Period: 26 February to 9 August 2021							
	February	March	April	May	June	July	August	Total
	(n = 3)	(n = 31)	(n = 30)	(n = 31)	(n = 30)	(n = 31)	(n = 9)	(n = 165)
ET_{0-PM} (mm)	11.7	179.0	191.3	214.4	196.7	187.8	49.1	1030.0
ET_{0-HS} (mm)	13.2	154.8	180.8	200.3	195.5	179.6	48.7	972.9
ET_{0-BC} (mm)	12.5	141.3	152.1	171.7	172.2	170.9	48.8	869.5
ET_{0-PM_NP} (mm)	13.4	183.7	204.8	242.7	238.5	203.5	52.3	1138.9

However, when considering total ET_0 (whole study period) and the PM method, HS recorded an ET_0 value 5.5% lower vs. PM; BC, a value 15.6% lower; and PM_NP, 10.6% higher; therefore, HS was the equation that yielded values closest to the PM method. This is because HS considers temperature and radiation as the main energy sources that promote evapotranspiration [9,27].

The results in Table 4 indicate an overestimation of ET_0 relative to the value obtained with the PM_NP method during the study period. The magnitude of this overestimation is related to the accuracy of each variable and has been reported only when using NP (NASA-POWER) data and the PM method [52,53,72].

Table 5 summarizes the relationship between the climatic variables recorded by the AWS and those obtained from the NP platform during the study period, where wind speed (WS) and solar radiation (SR) showed a low and moderate relationship, respectively. This same behavior has been reported by some authors for WS [27,45,73] and SR [74]. By contrast, Tmax and RH recorded a high ratio, and Tmin recorded a very high ratio. Some authors reported similar R^2 values for Tmin, Tmax [58], and RH [27] to those obtained in the present study. WS was the variable that yielded the lowest R^2 . This highlights the multiple challenges in determining this variable; these include quality control of the measured data since improving this aspect may return more accurate estimates [75].

Table 5. Relationship between the meteorological variables recorded by the automated weather station (AWS) and obtained from the NP platform during the study period.

Climatic Variables	Coefficient of Determination (R^2)				
	Tmax_NP	Tmin_NP	RH_NP	WS_NP	SR_NP
Tmax_AWS	0.76				
Tmin_AWS		0.81			
RH_AWS			0.80		
WS_AWS				0.27	
SR_AWS					0.45

Tmax, maximum temperature; Tmin, minimum temperature; RH, relative humidity; WS, wind speed; SR, solar radiation.

Figure 4 depicts the bias in the data recorded by the automated weather station (AWS) relative to NP platform data for the following meteorological variables: temperature (maximum and minimum), relative humidity, solar radiation, and wind speed. It is observed that 44% of the maximum temperature data evaluated ($n = 165$) were virtually unbiased, while 39% of NP data overestimated Tmax by 2.1 °C to 7.5 °C, and the rest of the data (17%) underestimated Tmax by 1.2 °C to 5.5 °C (Figure 4a). Regarding the minimum temperature,

39% of the data evaluated showed bias values close to zero, while 46% of the NP data overestimated Tmin by 1.6 °C to 5.1 °C and the rest (15%) underestimated Tmin by 1.8 °C to 5.3 °C (Figure 4b).

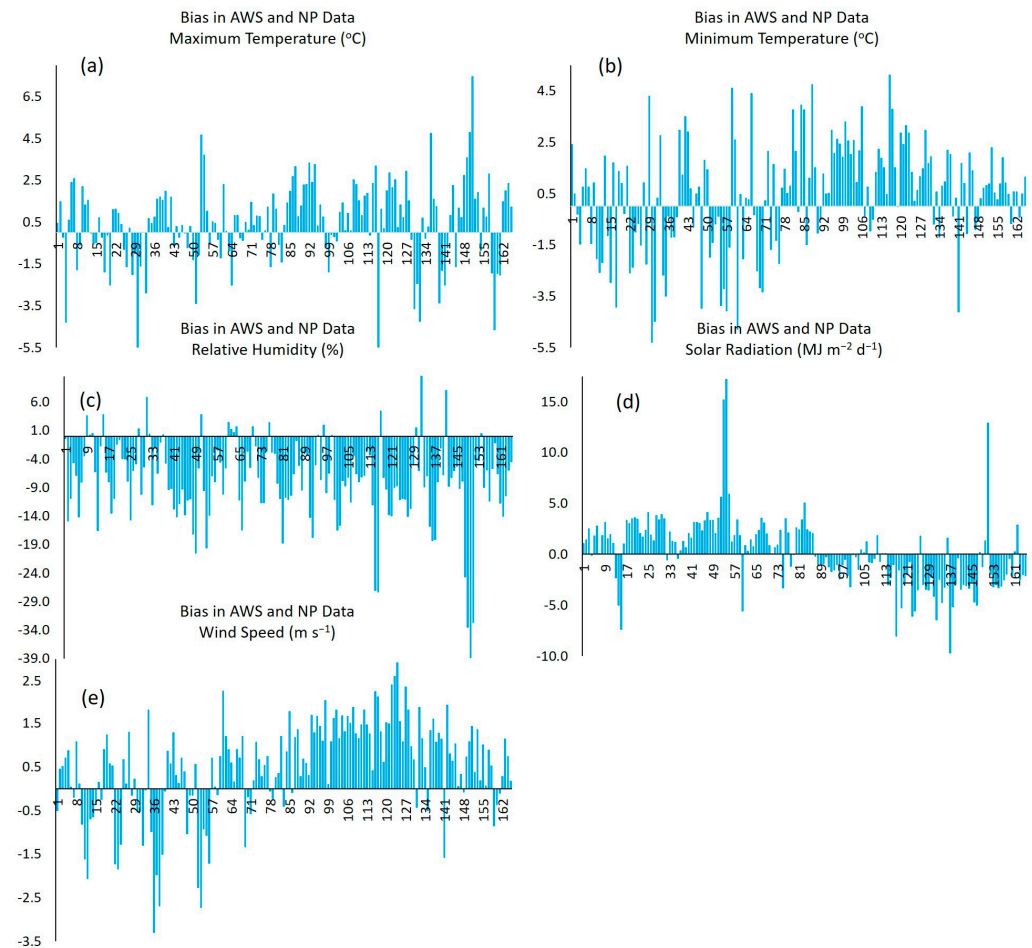


Figure 4. Bias between observed (AWS) and reference (NP) data for the meteorological. (a) Bias in AWS and NP Data Tmax. (b) Bias in AWS and NP Data Tmin. (c) Bias in AWS and NP Data RH. (d) Bias in AWS and NP Data SR. (e) Bias in AWS and NP Data WS.

The less biased RH values (values close to zero) were observed in 16% of the evaluated data; the NP platform underestimated RH by 3.0% to 38.8% in 76% of the data, and the rest of the data (7%) overestimated RH by 5.9% to 14.9% (Figure 4c). On the other hand, 45% of the evaluated data showed the minimum differences in solar radiation bias (values between 0 MJ m⁻² d⁻¹ and 1.5 MJ m⁻² d⁻¹), while 36% of the data overestimated radiation by 3.7 MJ m⁻² d⁻¹ to 17.2 MJ m⁻² d⁻¹, and the rest of the data (19%) underestimated radiation by 2.9 MJ m⁻² d⁻¹ to 9.7 MJ m⁻² d⁻¹ (Figure 4d).

Finally, 50% of the WS data showed bias values close to zero. It is also observed that most data (41%) overestimated WS by 1.4 m s⁻¹ to 2.9 m s⁻¹, and the rest of the data (9%) underestimated WS by 1.2 m s⁻¹ to 3.3 m s⁻¹ (Figure 4e).

Based on the above, the NP platform tends to overestimate Tmax, Tmin, SR, and WS while it underestimates RH. This same behavior was reported by Jiménez et al., in the study area for Tmin, WS, and RH [27].

Estimating the 5-day cumulative ET₀ improved the values of R², r, and c relative to daily ET₀ and 5-day mean ET₀. This behavior is consistent with the one reported by Jiménez et al. [27], who obtained better R² and RMSE values when estimating 10-day mean ET₀ versus daily data. Also, this way of estimating ET₀ yielded reliability coefficients (c) rated as “very good” for BC and PM_NP and “good” for HS. However, PM_NP showed

the best R^2 , r , and c values, while HS yielded the best RMSE, PE, MBE, and b (Table 6). The latter parameter returned values close to 1, indicating that the estimated values are statistically similar to observed or reference values [16]. Some authors reported similar RMSE values (1.1 mm d^{-1}) when comparing ET_0 estimated by the HS equation and the PM method on a daily basis [71,76]. However, some authors recorded an RMSE (0.7 mm d^{-1}) for 10-day mean data, which is similar to the RMSE value obtained in the present study for 5-day cumulative ET_0 [27].

Table 6. Comparison and inferential parameters to determine the ET_0 equation that best fits the study area.

Parameter	Methods								
	HS	BC	PM_NP	HS	BC	PM_NP	HS	BC	PM_NP
	Daily ET_0 ($n = 165$)			5-Day Mean ET_0 ($n = 33$)			5-Day Cumulative ET_0 ($n = 33$)		
R^2 (Dimensionless)	0.29	0.43	0.53	0.44	0.47	0.73	0.69	0.76	0.84
RMSE (mm d^{-1})	1.1	1.3	1.2	0.7	1.1	0.9	3.8	5.8	4.6
PE (%)	5.5	15.6	10.6	5.2	15.3	10.6	5.5	15.6	10.6
MBE (mm d^{-1})	−0.35	−0.97	0.66	−0.32	−0.95	0.66	−1.73	−4.86	3.30
d (Dimensionless)	0.94	0.99	0.98	0.85	1.00	0.94	0.86	1.00	0.94
r (Dimensionless)	0.54	0.65	0.73	0.66	0.69	0.85	0.83	0.87	0.91
c (Dimensionless)	0.51	0.65	0.72	0.56	0.66	0.81	0.71	0.83	0.86
b (Dimensionless)	0.9270	0.8257	1.0994	0.9416	0.8399	1.1073	0.9362	0.8349	1.1075

When graphically comparing the empirical equations versus the reference method (PM), daily ET_0 and 5-day mean ET_0 show a greater variability (Figure 5a,b); the 5-day cumulative ET_0 returned the best fit, with a lower variability of ET_0 values between the empirical equations and the PM method (Figure 5c).

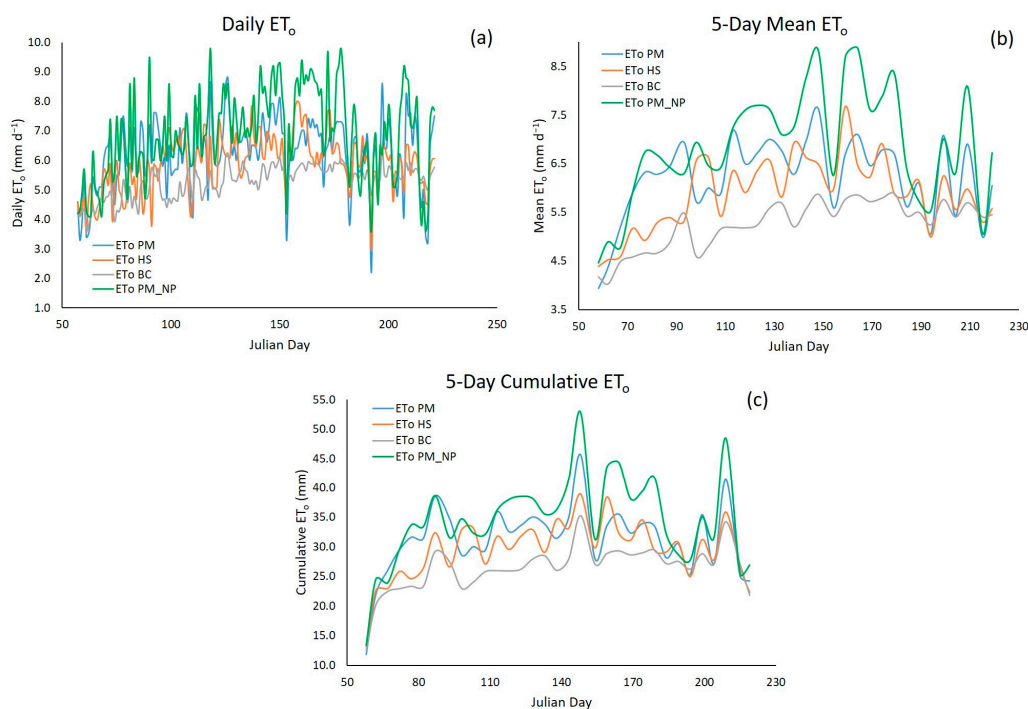


Figure 5. Different ways to estimate ET_0 using empirical equations and the reference method (PM) during the study period. (a) Estimation Daily ET_0 . (b) Estimation 5-Day Mean ET_0 . (c) Estimation 5-Day Cumulative ET_0 .

In addition, HS yielded a better fit than the reference method (PM) in the three ways of estimating ET_0 . Other authors have also reported a better fit with the HS equation relative to other methods and have taken PM as a reference for arid and semi-arid regions [16,35,76]. This equation underestimates ET_0 over most of the study period because the methods based on solar temperature and radiation do not include wind speed [19].

3.2. Comparison of Estimated ET_0 with Observed (AWS) versus Estimated (NP) Data

Table 7 shows the results of the goodness-of-fit tests between ET_0 calculated by the PM, HS, and BC methods, using maximum and minimum temperature data from the NP platform for the different calculation periods (daily, 5-day mean, and 5-day cumulative). The analyses of variance, with a 95% confidence interval (p -value < 0.0001), indicate a significant linear relationship between the PM method and the HS_{NP} and BC_{NP} equations for the three calculation periods. HS_{NP} yielded the best values of inferential parameters versus BC_{NP}, except for R^2 and r , in the daily ET_0 estimate. This indicates that HS with NP temperature data is a suitable option for estimating ET_0 for different periods. In addition, we found that the estimation percent error (PE) is lower than 5% with HS_{NP} for the three ET_0 calculation periods. In addition, MBE is negative in the three periods, pointing to an underestimation with the HS_{NP} method. Some authors report this same ET_0 underestimation effect in semi-arid regions during the winter–summer period [27,71].

Table 7. Comparison and linear regression coefficients between ET_0 calculated with the reference method (FAO-56 Penman–Monteith) and HS and BC methods with temperature data from the NP platform.

Parameter	Methods					
	HS _{NP}	BC _{NP}	HS _{NP}	BC _{NP}	HS _{NP}	BC _{NP}
	Daily ET_0 ($n = 165$)		5-Day Mean ET_0 ($n = 33$)		5-Day Cumulative ET_0 ($n = 33$)	
R^2 (Dimensionless)	0.29	0.38	0.55	0.45	0.75	0.74
RMSE (mm d ⁻¹)	1.1	1.3	0.6	1.1	3.3	5.7
PE (%)	4.4	15.0	4.1	14.6	4.4	15.0
MBE (mm d ⁻¹)	−0.28	−0.93	−0.26	−0.91	−1.38	−4.67
r (Dimensionless)	0.54	0.61	0.74	0.67	0.87	0.86
a (Dimensionless)	2.435	−0.359	1.623	0.732	2.647	−1.700
b (Dimensionless)	0.638	1.244	0.770	1.033	0.957	1.240

The 5-day mean ET_0 estimate recorded the best values in most statistical parameters relative to the mean daily ET_0 . However, the 5-day cumulative ET_0 estimate recorded the best r and R^2 values compared with the other two estimates (daily ET_0 and 5-day mean ET_0). These good results are obtained because grouping ET_0 over five days mitigates the variation in daily temperature associated with precipitation, wind speed, and cloudiness [77].

Figure 6 shows the dispersion of the calibrated HS method (HS_{cal}) relative to PM for the different ET_0 calculation periods, depicting the best data fit obtained using data accumulated over five days.

The comparison of ET_0 estimates with the HS equation using temperature data recorded by the AWS (HS_{AWS}) and from the NP platform (HS_{NP}) yielded a high correlation for the three estimates (Figure 7); the 5-day cumulative ET_0 recorded the highest R^2 . These R^2 values indicate the feasibility of estimating ET_0 using the NP platform's temperature data and the HS formula [27,71,76].

The accuracy of ET_0 calculated with methods BC and HS was compared versus the FAO-56 Penman–Monteith (PM) reference method using data from an automated weather station (AWS) and the NASA-POWER platform (NP). In this comparison, the HS equation returned the best fit in the different ways of estimating ET_0 : daily, 5-day mean, and 5-day cumulative, with the latter yielding the best fit.

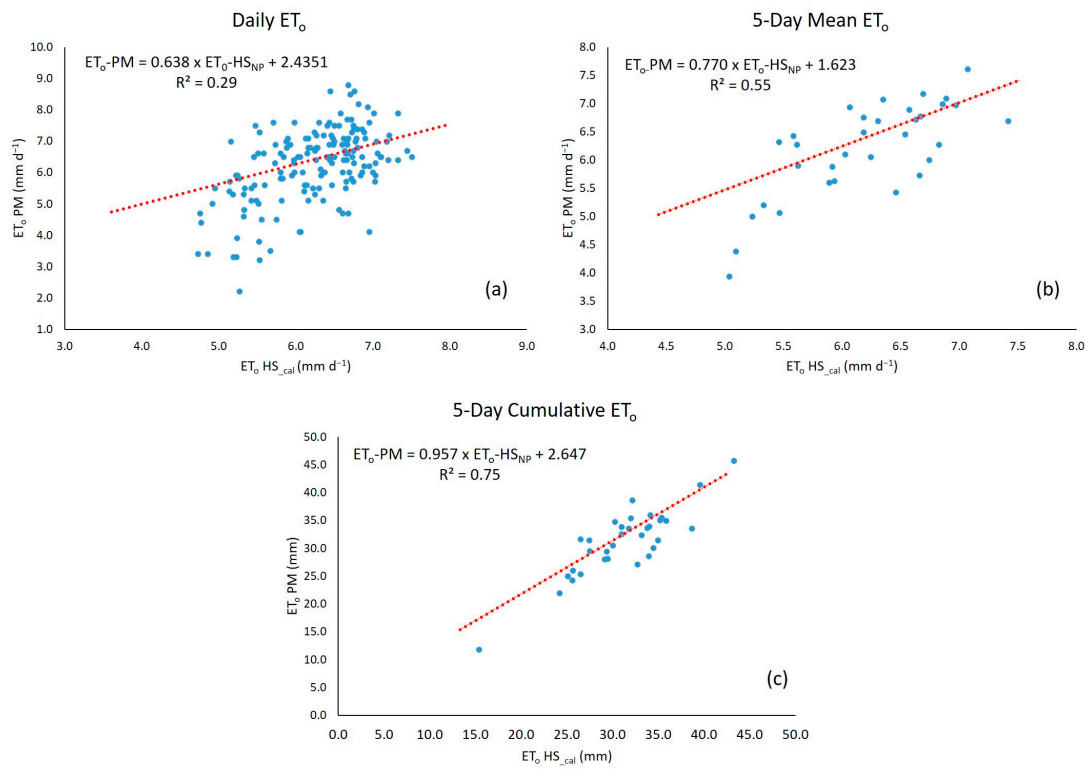


Figure 6. Dispersion plot of the calibrated HS method (HS_{NP}) relative to the FAO-56 Penman-Monteith (PM) reference method for the different ET₀ calculation periods: Daily (a), 5-Day Mean (b) 5-Day Cumulative (c).

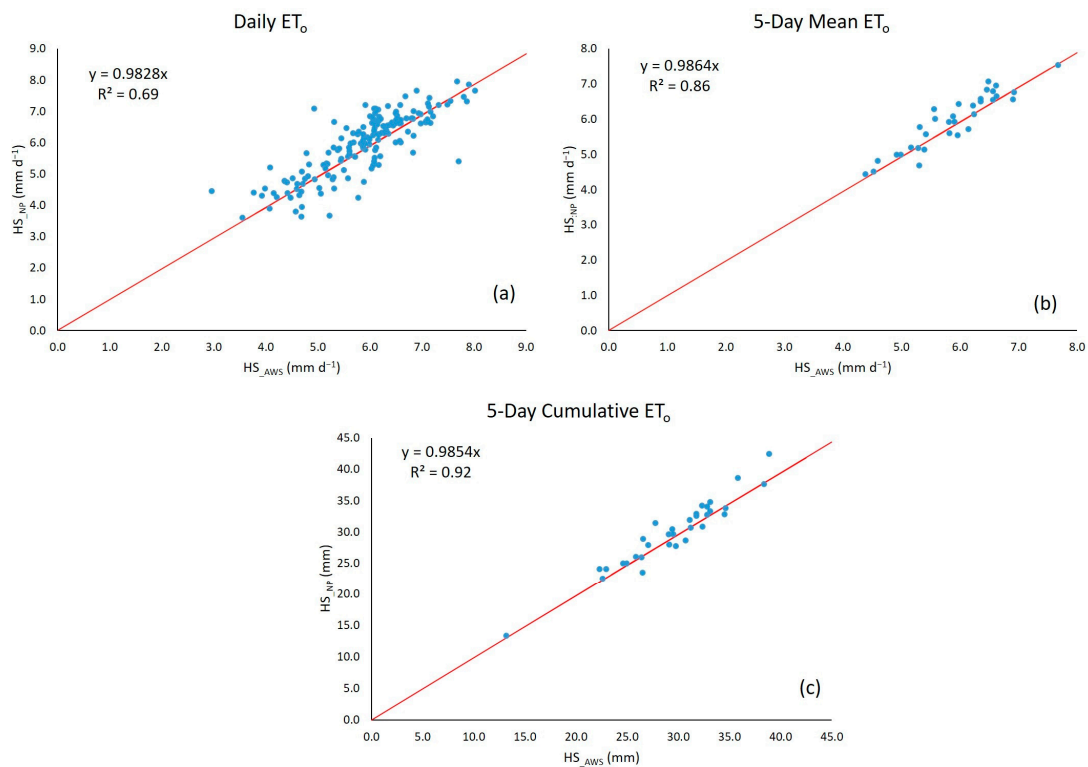


Figure 7. Linear relationship between ET₀ estimates with the HS equation using temperature data from the AWS and the NP platform for the different ET₀ calculation periods: Daily (a), 5-Day Mean (b) 5-Day Cumulative (c).

4. Conclusions

The Hargreaves–Samani (HS) method underestimated by 5.5% the reference evapotranspiration (ET_0) compared to the FAO-56 Penman–Monteith (PM) method considering the total ET_0 of the study period (26 February to 9 August 2021). This was because the calculation of ET_0 with the HS equation does not consider wind speed, which influences the evapotranspiration rate sometimes during the year in the study area. Nonetheless, this method is an alternative for calculating ET_0 in semi-arid regions for which only temperature records are available.

The HS equation yielded the best estimate relative to the reference method (PM) in the different ways of estimating ET_0 during the spring–summer crop cycle; the 5-day cumulative ET_0 showed the best fit. Therefore, this method is suitable for use with remote-sensing data to determine crop evapotranspiration (ET_c) with 5-day temporal resolution images. It is necessary to conduct testing of HS in various agroclimatic conditions and perform a regional spatial evaluation using data from additional automated weather stations, such as those located within the entire 017 irrigation district.

The maximum and minimum temperature data from the NASA–POWER (NP) platform was suitable for estimating ET_0 with the HS equation. This data source is a timely alternative, particularly in semi-arid regions without data from weather stations.

The results showed that NP is a reliable data source for programming medium- and low-frequency irrigation (sprinkler and surface irrigation), which are common in the study area. In addition, they provide spatially comprehensive data, unlike the point values recorded by weather stations, which could be an enormous advantage when studying large regions, such as irrigation districts.

Author Contributions: Conceptualization, M.A.B.-G. and G.D.-R.; methodology, M.A.B.-G., G.D.-R. and A.Q.-N.; formal analysis, M.A.B.-G. and G.D.-R.; research, M.A.B.-G., G.D.-R. and A.L.-P.; preparation of the original draft, G.D.-R.; writing, review, and editing, M.A.B.-G., A.Q.-N., A.L.-P. and J.E.-Á.; supervision, M.A.B.-G. All authors have read and agreed to the published version of the manuscript.

Funding: This research received no external funding.

Institutional Review Board Statement: Not applicable.

Informed Consent Statement: Not applicable.

Data Availability Statement: The data are not publicly available because they are currently used in an ongoing thesis.

Acknowledgments: To the Consejo Nacional de Ciencia y Tecnología (National Council of Science and Technology, CONACYT) for financing the Ph.D. studies of G.D.-R. (Scholarship no. 765686) and to the GIS Water and Soil Laboratory at CENID-RASPA INIFAP for the use of the Automated Weather Station (AWS). María Elena Sánchez-Salazar translated the manuscript into English.

Conflicts of Interest: The authors declare that they have no conflict of interest.

References

1. Irmak, S. Evapotranspiration. In *Encyclopedia of Ecology*; Academic Press: Cambridge, MA, USA, 2008; pp. 1432–1438. [[CrossRef](#)]
2. Stanhill, G. Evapotranspiration. In *Reference Module in Earth Systems and Environmental Sciences*; Elsevier: Amsterdam, The Netherlands, 2019. [[CrossRef](#)]
3. Singh, P.; Srivastava, P.K.; Mall, R.K. Estimation of potential evapotranspiration using INSAT-3D satellite data over an agriculture area. *Agric. Water Manag.* **2021**, *2021*, 143–155. [[CrossRef](#)]
4. Melesse, A.M.; Weng, Q.; Thenkabail, P.S.; Senay, G.B. Remote Sensing Sensors and Applications in Environmental Resources Mapping and Modelling. *Sensors* **2007**, *7*, 3209–3241. [[CrossRef](#)]
5. Chaudhary, S.K.; Srivastava, P.K. Future challenges in agricultural water management. *Agric. Water Manag.* **2021**, *2021*, 445–456. [[CrossRef](#)]
6. Huntington, T.G. Climate Warming-Induced Intensification of the Hydrologic Cycle. *Adv. Agron.* **2010**, *109*, 1–53. [[CrossRef](#)]
7. Wang, L.; Iddio, E.; Ewers, B. Introductory overview: Evapotranspiration (ET) models for controlled environment agriculture (CEA). *Comput. Electron. Agric.* **2021**, *190*, 106447. [[CrossRef](#)]

8. Althoff, D.; Rodrigues, L.N. Improvement of reference crop evapotranspiration estimates using limited data for the Brazilian Cerrado. *Sci. Agric.* **2023**, *80*, 1–11. [[CrossRef](#)]
9. Allen, R.G.; Pereira, L.; Raes, D.; Smith, M. *Crop Evapotranspiration: Guidelines for Computing Crop Requirements*; Irrigation and Drainage paper No. 56; FAO: Rome, Italy, 1998; Available online: <https://www.fao.org/3/x0490e/x0490e00.htm> (accessed on 1 March 2022).
10. Gong, L.; Xu, C.; Chen, D.; Halldin, S.; Chen, Y.D. Sensitivity of the Penman-Monteith reference evapotranspiration to key climatic variables in the Changjiang (Yangtze River) basin. *J. Hydrol.* **2006**, *329*, 620–629. [[CrossRef](#)]
11. Pereira, L.S.; Alves, I.; Paredes, P. Crop and landscape water requirements. In *Reference Module in Earth Systems and Environmental Sciences*; Elsevier: Amsterdam, The Netherlands, 2022. [[CrossRef](#)]
12. Peng, L.; Li, Y.; Feng, H. The best alternative for estimating reference crop evapotranspiration in different sub-regions of mainland China. *Sci. Rep.* **2017**, *7*, 5458. [[CrossRef](#)]
13. Talebmorad, H.; Ahmadnejad, A.; Eslamian, S.; Askari, K.O.A.; Singh, V.P. Evaluation of uncertainty in evapotranspiration values by FAO56-Penman-Monteith and Hargreaves-Samani methods. *Int. J. Hydrol. Sci. Technol.* **2020**, *10*, 135–147. [[CrossRef](#)]
14. Wen, C.; Shuanghe, S.H.; Chunfeng, D. Sensitivity of the Penman-Monteith Reference Evapotranspiration in Growing Season in the Northwest China. In Proceedings of the International Conference on Multimedia Technology, Ningbo, China, 29–31 October 2010. [[CrossRef](#)]
15. Muhammad, M.K.I.; Shahid, S.; Ismail, T.; Harun, S.; Kisi, O.; Yaseen, Z.M. The development of evolutionary computing model for simulating reference evapotranspiration over Peninsular Malaysia. *Theor. Appl. Clim.* **2021**, *144*, 1419–1434. [[CrossRef](#)]
16. Raziie, T.; Pereira, L.S. Estimation of ETo with Hargreaves-Samani and FAO-PM temperature methods for a wide range of climates in Iran. *Agric. Water Manag.* **2013**, *121*, 1–18. [[CrossRef](#)]
17. Gabr, M.E.-S. Management of irrigation requirements using FAO-CROPWAT 8.0 model: A case study of Egypt. *Model. Earth Syst. Environ.* **2022**, *8*, 3127–3142. [[CrossRef](#)]
18. Surendran, U.; Sushanth, C.M.; Joseph, E.J.; Al-Ansari, N.; Yaseen, Z.M. FAO CROPWAT Model-Based Irrigation Requirements for Coconut to Improve Crop and Water Productivity in Kerala, India. *Sustainability* **2019**, *11*, 5132. [[CrossRef](#)]
19. Ortiz, R.S.; Chile, A.M. Métodos de cálculo para estimar la evapotranspiración de referencia para el Valle de Tumbaco. *Siembra* **2020**, *7*, 70–79. [[CrossRef](#)]
20. Yamaç, S.S. Reference Evapotranspiration Estimation With kNN and ANN Models Using Different Climate Input Combinations in the Semi-arid Environment. *J. Agric. Sci. Tarim Bilimleri Dergisi* **2021**, *27*, 129–137. [[CrossRef](#)]
21. Sahoo, B.; Walling, I.; Deka, B.C.; Bhatt, B.P. Standardization of Reference Evapotranspiration Models for a Subhumid Valley Rangeland in the Eastern Himalayas. *J. Irrigat. Drain. Eng.* **2012**, *138*, 880–895. [[CrossRef](#)]
22. Srivastava, A.; Sahoo, B.; Raghuvanshi, N.S.; Singh, R. Evaluation of Variable-Infiltration Capacity Model and MODIS-Terra Satellite-Derived Grid-Scale Evapotranspiration Estimates in a River Basin with Tropical Monsoon-Type Climatology. *J. Irrig. Drain. Eng.* **2017**, *143*, 04017028. [[CrossRef](#)]
23. Allen, R.G.; Pereira, L.S.; Raes, D.; Smith, M. Evapotranspiración del cultivo: Guías para la determinación de los requerimientos de agua de los cultivos. In *FAO Riego y Drenaje Manual 56*; FAO: Rome, Italy, 2006; Available online: <https://www.fao.org/3/x0490s/x0490s00.htm> (accessed on 15 May 2022).
24. Gavilán, M.P.; Estévez, J.; Berengena, J. ETo estandarizada en el sur de España ¿Cuál debe ser la referencia? In Proceedings of the XXXIV Congreso Nacional de Riegos, Escuela Universitaria de Ingeniería Técnica Agrícola, Sevilla, Spain, 7–9 June 2016; Available online: <https://idus.us.es/bitstream/handle/11441/41070/T-A-01.pdf?sequence=1&isAllowed=y> (accessed on 23 July 2023).
25. Borges, J.C.F.; Anjos, R.J.; Silva, T.J.A.; Lima, J.R.S.; Andrade, C.L.T. Métodos de estimativa da evapotranspiração de referência diária para a microrregião de Garanhuns, PE. *Rev. Bras. Eng. Agrí Amb.* **2012**, *16*, 380–390. [[CrossRef](#)]
26. Woldesenbet, T.A.; Elagib, N.A. Spatial-temporal evaluation of different reference evapotranspiration methods based on the climate forecast system reanalysis data. *Hydrol. Process.* **2021**, *36*, e14239. [[CrossRef](#)]
27. Jiménez, J.S.I.; Ojeda, B.W.; Inzunza, I.M.A.; Marcial, P.M.D.J. Analysis of the NASA-POWER system for estimating reference evapotranspiration in the Comarca Lagunera, Mexico. *Ing. Agrícola Biosist.* **2021**, *13*, 201–226. [[CrossRef](#)]
28. Luo, Y.; Chang, X.; Peng, S.; Khan, S.; Wang, W.; Zheng, Q.; Cai, X. Short-term forecasting of daily reference evapotranspiration using the Hargreaves-Samani model and temperature forecasts. *Agric. Water Manag.* **2014**, *136*, 42–51. [[CrossRef](#)]
29. Perera, K.C.; Western, A.W.; Nawarathna, B.; George, B. Forecasting daily reference evapotranspiration for Australia using numerical weather prediction outputs. *Agric. For. Meteorol.* **2014**, *194*, 50–63. [[CrossRef](#)]
30. Xiong, Y.; Luo, Y.; Wang, Y.; Traore, S.; Xu, J.; Jiao, X.; Fipps, G. Forecasting daily reference evapotranspiration using the Blaney-Criddle model and temperature forecasts. *Arch. Agron. Soil. Sci.* **2015**, *62*, 790–805. [[CrossRef](#)]
31. Goh, E.H.; Ng, J.L.; Huang, Y.F.; Yong, S.L.S. Performance of potential evapotranspiration models in Peninsular Malaysia. *J. Water Clim. Chang.* **2021**, *12*, 3170–3186. [[CrossRef](#)]
32. Fooladmand, H.R. Evaluation of some equations for estimating evapotranspiration in the south of Iran. *Arch. Agron. Soil. Sci.* **2011**, *57*, 741–752. [[CrossRef](#)]
33. Hafeez, M.; Ahmad, C.Z.; Akhtar, K.A.; Bakhsh, G.A.; Basit, A.; Tahira, F. Comparative Analysis of Reference Evapotranspiration by Hargreaves and Blaney-Criddle Equations in Semi-Arid Climatic Conditions. *Curr. Res. Agric. Sci.* **2020**, *7*, 52–57. [[CrossRef](#)]

34. Martinez, C.J.; Thepadia, M. Estimating Reference Evapotranspiration with Minimum Data in Florida. *J. Irrig. Drain. Eng.* **2010**, *136*, 494–501. [[CrossRef](#)]
35. Tabari, H. Evaluation of Reference Crop Evapotranspiration Equations in Various Climates. *Water Resour. Manag.* **2010**, *24*, 2311–2337. [[CrossRef](#)]
36. Lima, J.R.d.S.; Antonino, A.C.D.; Souza, E.S.d.; Hammecker, C.; Montenegro, S.M.G.L.; Lira, C.A.B.d.O. Calibration of Hargreaves-Samani Equation for Estimating Reference Evapotranspiration in Sub-Humid Region of Brazil. *J. Water Resour. Prot.* **2013**, *5*, 1–5. [[CrossRef](#)]
37. Temesgen, B.; Eching, S.; Davidoff, B.; Frame, K. Comparison of Some Reference Evapotranspiration Equations for California. *J. Irrig. Drain. Eng.* **2005**, *131*, 73–84. [[CrossRef](#)]
38. Todorovic, M.; Karic, B.; Pereira, L.S. Reference evapotranspiration estimate with limited weather data across a range of Mediterranean climates. *J. Hydrol.* **2013**, *481*, 166–176. [[CrossRef](#)]
39. Shahidian, S.; Serralheiro, R.P.; Serrano, J.; Teixeira, J.L. Parametric calibration of the Hargreaves-Samani equation for use at new locations. *Hydrol. Process.* **2012**, *27*, 605–616. [[CrossRef](#)]
40. Sepaskhah, A.R.; Razzaghi, F. Evaluation of the adjusted Thornthwaite and Hargreaves-Samani methods for estimation of daily evapotranspiration in a semi-arid region of Iran. *Arch. Agron. Soil. Sci.* **2009**, *55*, 51–66. [[CrossRef](#)]
41. Hafeez, M.; Chatha, Z.A.; Bakhsh, A.; Basit, A.; Khan, A.A.; Tahira, F. Reference Evapotranspiration by Hargreaves and Modified Hargreaves Equations under Semi-Arid Environment. *Curr. Res. Agric. Sci.* **2020**, *7*, 58–63. [[CrossRef](#)]
42. Martins, D.S.; Paredes, P.; Raziqi, T.; Pires, C.; Cadima, J.; Pereira, L.S. Assessing reference evapotranspiration estimation from reanalysis weather products. An application to the Iberian Peninsula. *Int. J. Climatol.* **2016**, *37*, 2378–2397. [[CrossRef](#)]
43. Paredes, P.; Martins, D.S.; Pereira, L.S.; Cadima, J.; Pires, C. Accuracy of daily estimation of grass reference evapotranspiration using ERA-Interim reanalysis products with assessment of alternative bias correction schemes. *Agric. Water Manag.* **2018**, *210*, 340–353. [[CrossRef](#)]
44. Pelosi, A.; Terribile, F.; D’Urso, G.; Chirico, G. Comparison of ERA5-Land and UERRA MESCAN-SURFEX Reanalysis Data with Spatially Interpolated Weather Observations for the Regional Assessment of Reference Evapotranspiration. *Water* **2020**, *12*, 1669. [[CrossRef](#)]
45. Rodrigues, G.C.; Braga, R.P. Evaluation of NASA POWER Reanalysis Products to Estimate Daily Weather Variables in a Hot Summer Mediterranean Climate. *Agronomy* **2021**, *11*, 1207. [[CrossRef](#)]
46. Park, J.; Choi, M. Estimation of evapotranspiration from ground-based meteorological data and global land data assimilation system (GLDAS). *Stoch. Environ. Res. Risk Assess.* **2015**, *29*, 1963–1992. [[CrossRef](#)]
47. Tian, D.; Martinez, C.J.; Graham, W.D. Seasonal Prediction of Regional Reference Evapotranspiration Based on Climate Forecast System Version 2. *J. Hydrometeorol.* **2014**, *15*, 1166–1188. [[CrossRef](#)]
48. Peters, L.C.D.; Kumar, S.V.; Mocko, D.M.; Tian, Y. Estimating evapotranspiration with land data assimilation systems. *Hydrol. Process.* **2011**, *25*, 3979–3992. [[CrossRef](#)]
49. McEvoy, D.J.; Roj, S.; Dunkerly, C.; McGraw, D.; Huntington, J.L.; Hobbins, M.T.; Ott, T. Validation and Bias Correction of Forecast Reference Evapotranspiration for Agricultural Applications in Nevada. *J. Water Resour. Plan. Manag.* **2022**, *148*, 04022057. [[CrossRef](#)]
50. Blankenau, P.A.; Kilic, A.; Allen, R. An evaluation of gridded weather data sets for the purpose of estimating reference evapotranspiration in the United States. *Agric. Water Manag.* **2020**, *242*, 106376. [[CrossRef](#)]
51. Ndiaye, P.M.; Bodian, A.; Diop, L.; Deme, A.; Dezetter, A.; Djaman, K.; Ogilvie, A. Trend and Sensitivity Analysis of Reference Evapotranspiration in the Senegal River Basin Using NASA Meteorological Data. *Water* **2020**, *12*, 1957. [[CrossRef](#)]
52. Negm, A.; Jabro, J.; Provenzano, G. Assessing the suitability of American National Aeronautics and Space Administration (NASA) agro-climatology archive to predict daily meteorological variables and reference evapotranspiration in Sicily, Italy. *Agric. For. Meteorol.* **2017**, *244–245*, 111–121. [[CrossRef](#)]
53. Srivastava, P.K.; Singh, P.; Mall, R.K.; Pradhan, R.K.; Bray, M.; Gupta, A. Performance assessment of evapotranspiration estimated from different data sources over agricultural landscape in Northern India. *Theor. Appl. Clim.* **2020**, *140*, 145–156. [[CrossRef](#)]
54. Rodrigues, G.C.; Braga, R.P. Estimation of Daily Reference Evapotranspiration from NASA POWER Reanalysis Products in a Hot Summer Mediterranean Climate. *Agronomy* **2021**, *11*, 2077. [[CrossRef](#)]
55. Davis. Instrumentos Climáticos de Precisión. Catálogo Global. 2020. Available online: https://cdn.shopify.com/s/files/1/0515/5992/3873/files/Weather_Catalog_Spanish.pdf (accessed on 10 February 2020).
56. Instituto Nacional de Estadística y Geografía (INEGI). Continuo de Elevaciones Mexicano (CEM 3.0), Coahuila. 2013. Available online: <https://www.inegi.org.mx/app/geo2/elevacionesmex/> (accessed on 19 July 2023).
57. Instituto Nacional de Estadística y Geografía (INEGI). Uso de Suelo y Vegetación, Conjunto de Datos Vectoriales de Uso del Suelo y Vegetación. Escala 1:250 000. Serie VII. 2018. Available online: <https://www.inegi.org.mx/temas/ususuelo/> (accessed on 21 July 2023).
58. White, J.W.; Hoogenboom, G.; Stackhouse, P.W.; Hoell, J.M. Evaluation of NASA satellite- and assimilation model-derived long-term daily temperature data over the continental US. *Agric. For. Meteorol.* **2008**, *148*, 1574–1584. [[CrossRef](#)]
59. Zhang, T.; Chandler, W.S.; Hoell, J.M.; Westberg, D.; Whitlock, C.H.; Stackhouse, P.W. A Global Perspective on Renewable Energy Resources: Nasa’s Prediction of Worldwide Energy Resources (Power) Project. In Proceedings of the ISES World Congress 2007, Beijing, China, 18–21 September 2007; Springer: Berlin/Heidelberg, Germany, 2007; Volumes 1–5, pp. 2636–2640. [[CrossRef](#)]

60. Monteiro, L.A.; Sentelhas, P.C.; Pedra, G.U. Assessment of NASA/POWER satellite-based weather system for Brazilian conditions and its impact on sugarcane yield simulation. *Int. J. Climatol.* **2017**, *38*, 1571–1581. [CrossRef]
61. Zhang, T.; Stackhouse, P.W.; Gupta, S.K.; Cox, S.J.; Mikovitz, J.C. Validation and Analysis of the Release 3.0 of the NASA GEWEX Surface Radiation Budget Dataset. *AIP Conf. Proc.* **2009**, *1100*, 597–600. [CrossRef]
62. National Aeronautics and Space Administration. Prediction of Worldwide Energy Resource. 2023. Available online: <https://power.larc.nasa.gov/> (accessed on 18 March 2023).
63. Allen, R.G.; Pruitt, W.O.; Businger, J.A.; Fritschen, L.J.; Jensen, M.E.; Quinn, F.H. Capítulo 4 Evaporation and Transpiration. In *ASCE Handbook of Hydrology*; American Society of Civil Engineers: Reston, VA, USA, 1996; pp. 125–252. [CrossRef]
64. Hargreaves, G.H.; Samani, Z.A. Reference crop evapotranspiration from ambient air temperature. *Appl. Eng. Agric.* **1985**, *1*, 96–99. [CrossRef]
65. Chávez, R.E.; González, C.G.; González, B.J.L.; Dzul, L.E.; Sánchez, C.I.; López, S.A.; Chávez, S.J.A. Uso de estaciones climatológicas automáticas y modelos matemáticos para determinar la evapotranspiración. *Tecnol. Cienc. Agua* **2013**, *4*, 115–126. Available online: <https://www.scielo.org.mx/pdf/tca/v4n4/v4n4a7.pdf> (accessed on 23 June 2022).
66. Doorenbos, J.; Pruitt, W.O. *Guidelines for Predicting Crop Water Requirements*; Irrigation and Drainage Paper FAO-24; FAO: Rome, Italy, 1977; Available online: <https://www.fao.org/publications/card/en/c/6bae3071-5d7b-5206-af5c-c9bfa1d9d1fe/> (accessed on 29 May 2022).
67. Silva, G.H.d.; Dias, S.H.B.; Ferreira, L.B.; Santos, J.É.O.; Cunha, F.F.d. Performance of different methods for reference evapotranspiration estimation in Jaíba, Brazil. *Rev. Bras. Eng. Agric. Amb.* **2018**, *22*, 83–89. [CrossRef]
68. Debnath, S.; Adamala, S.; Raghuwanshi, N.S. Sensitivity Analysis of FAO-56 Penman-Monteith Method for Different Agro-ecological Regions of India. *Environ. Process.* **2015**, *2*, 689–704. [CrossRef]
69. Jerszurki, D.; de Souza, J.L.M.; Ramos, S.L.d.C. Sensitivity of ASCE-Penman-Monteith reference evapotranspiration under different climate types in Brazil. *Clim. Dyn.* **2019**, *53*, 943–956. [CrossRef]
70. Ndiaye, P.M.; Bodian, A.; Diop, L.; Djaman, K. Sensitivity Analysis of the Penman-Monteith Reference Evapotranspiration to Climatic Variables: Case of Burkina Faso. *J. Water Resour. Prot.* **2017**, *9*, 1364–1376. [CrossRef]
71. Villa, C.A.O.; Ontiveros, C.R.E.; Ruíz, A.O.; González, S.A.; Quevedo, T.J.A.; Ordoñez, H.L.M. Spatio-temporal variation of reference evapotranspiration from empirical methods in Chihuahua, Mexico. *Ing. Agrícola Biosist.* **2021**, *13*, 95–115. [CrossRef]
72. Maldonado, W.; Valeriano, T.T.B.; de Souza, R.G. EVAPO: A smartphone application to estimate potential evapotranspiration using cloud gridded meteorological data from NASA-POWER system. *Comput. Electron. Agric.* **2019**, *156*, 187–192. [CrossRef]
73. Duarte, Y.C.N.; Sentelhas, P.C. NASA/POWER and DailyGridded weather datasets—How good they are for estimating maize yields in Brazil? *Int. J. Biometeorol.* **2020**, *64*, 319–329. [CrossRef]
74. Quansah, A.D.; Dogbey, F.; Asilevi, P.J.; Boakye, P.; Darkwah, L.; Oduro, K.S.; Sokama, N.Y.A.; Mensah, P. Assessment of solar radiation resource from the NASA-POWER reanalysis products for tropical climates in Ghana towards clean energy application. *Sci. Rep.* **2022**, *12*, 10684. [CrossRef]
75. De Pondeca, M.S.F.V.; Manikin, G.S.; DiMego, G.; Benjamin, S.G.; Parrish, D.F.; Purser, R.J.; Wan, S.W.; Horel, J.D.; Myrick, D.T.; Lin, Y.; et al. The Real-Time Mesoscale Analysis at NOAA's National Centers for Environmental Prediction: Current Status and Development. *Weather Forecast.* **2011**, *26*, 593–612. [CrossRef]
76. Najmaddin, P.M.; Whelan, M.J.; Balzter, H. Estimating Daily Reference Evapotranspiration in a Semi-Arid Region Using Remote Sensing Data. *Remote Sens.* **2017**, *9*, 779. [CrossRef]
77. Teixeira, P.; Pannunzio, A.; Brenner, J. Calibración de la ecuación de Hargreaves para el cálculo de la evapotranspiración de cultivo de referencia (ET_o) en Salto, Uruguay. *Rev. Climatol.* **2021**, *21*, 80–88. Available online: <https://rclimatol.eu/wp-content/uploads/2021/06/Articulo21g.pdf> (accessed on 23 June 2023).

Disclaimer/Publisher's Note: The statements, opinions and data contained in all publications are solely those of the individual author(s) and contributor(s) and not of MDPI and/or the editor(s). MDPI and/or the editor(s) disclaim responsibility for any injury to people or property resulting from any ideas, methods, instructions or products referred to in the content.